2-2020

Cycle-to-cycle flow variations in a square duct with a symmetrically oscillating constriction

Erica Sherman

Lori M. Lambert

Bethany White

Michael H. Krane

Timothy Wei

HHS Public Access

Author manuscript

Fluid Dyn Res. Author manuscript; available in PMC 2021 May 26.

Published in final edited form as:

Fluid Dyn Res. 2020 February ; 52(1): . doi:10.1088/1873-7005/ab52bf.

Cycle-to-cycle flow variations in a square duct with a symmetrically oscillating constriction

Erica Sherman[1], **Lori Lambert**[1], **Bethany White**[1], **Michael H. Krane**[2], **Timothy Wei**[1,†]

[1]Dept. of Mechanical & Materials Eng'g.; University of Nebraska – Lincoln; Lincoln, NE 68588

[2]Applied Research Laboratory; Penn State University; State College, PA 16804

Abstract

Spatially and temporally resolved Digital Particle Image Velocimetry (DPIV) measurements are presented of flow complexities in a nominally two-dimensional, symmetric, duct with an oscillating constriction. The motivation for this research lies in advancing the state-of-the-art in applying integral control volume analysis to modeling unsteady internal flows. The specific target is acoustic modeling of human phonation. The integral mass and momentum equations are directly coupled to the acoustic equations and provide quantitative insight into acoustic source strengths in addition to the dynamics of the fluid-structure interactions in the glottis. In this study, a square cross-section duct was constructed with symmetric, computer controlled, oscillating constrictions that incorporate both rocking as well as oscillatory open/close motions. Experiments were run in a free-surface water tunnel over a Strouhal number range, based on maximum jet speed and model length, of 0.012 - 0.048, for a fixed Reynolds number, based on maximum gap opening and maximum jet speed, of 8000. In this study, the constriction motions were continuous with one open-close cycle immediately following another. While the model and its motions were nominally two-dimensional and symmetric, flow asymmetries and oscillation frequency dependent cycle-to-cycle variations were observed. These are examined in the context of terms in the integral conservation equations.

1. Introduction

1.1. Overview

Internal duct flows with time-varying constrictions are common in both natural and engineered systems. For instance, Chang (1994) examined the flow induced vibration of reeds in the context of seals and plugs in high power machinery. Hirschberg, *et al.* (1996), Fabre, *et al.* (2012), Vilain, *et al.* (2003) and Tarnopolsky, et al. (2000) studied sound production mechanisms from musical instruments. A physiological example with a much more three-dimensional geometry is human and prosthetic heart valves. This has been studied by Peskin (1982), Yoganathan, *et al.* (2005), Rashtian, *et al.* (1986) and Bach, *et al.* (2002), amongst many others. Another physiological example of a naturally occurring oscillatory constriction is mammalian phonation (voice production).

†corresponding author.

A common theme of all of these types of internal flows is the importance of understanding the dynamics of fully-coupled fluid-structure interactions. For machinery, the problem may be vibration and fatigue. For heart valves, the dynamics ultimately govern the patient's health and well-being. And for voice and musical instruments, the issue is sound quality. The challenge is to understand, model and ideally control time-varying force coupling between flow and passageway.

The focus of the present work is to advance and apply integral control volume analysis, developed in Benaroya & Wei (2000) and Krane (2013, 2019), to a dynamically rich flow in a symmetric, oscillating constriction geometry that mimics the principal motions of the human glottis during phonation. The specific goal of this paper is to leverage spatially and temporally resolved measurements in clinical, science-based, computational modeling of voice disorders. This is part of a joint computational-experimental effort where similar data analysis is being done computationally, Zhang & Yang (2016), Yang, et al. (2017), Yang, el al. (2018), Zhang, el al. (2019), and in life-scale physical models, McPhail et al. (2019).

To set the stage, this section begins with a brief review of the voice literature. This is followed by an overview of integral control volume analysis and a more detailed problem statement. For the purposes of this study, a more classical incompressible fluid dynamics perspective of control volumes is taken. But as in Krane (2013, 2019), the connectivity between the flow through the glottal model and acoustics is highlighted.

1.2. A Brief Review of the Voice Literature

Verbal communication has been a defining feature of human civilization for over ten thousand years. Ramig & Verdolini (1998) and Roy, et al. (2005) estimated that anywhere from 3% to 9% of people in the United States suffer from some type of voice abnormality. These conditions can have powerful effects beyond a person's physical health, reaching into the individual's ability to work and interface with society, thereby affecting the individual's mental and emotional wellbeing. For this reason, the ability to understand, model and ultimately restore the ability to speak remains critically important.

Voice production originates from the forcing of air through the glottis, the narrow gap in the airway between the vocal folds. Some of the energy from this pulsatile flowfield is released as sound. Understanding the fluid-structure interactions associated with phonation, then, can assist physicians and engineers in treating dysfunction as well as replicating human voice.

Accessibility to the vocal folds, *i.e.* the small size of the glottis, and the high frequencies of the vocal fold vibrations, continues to challenge experimenters interested in directly observing and quantifying phonation dynamics. There have been a variety of vocal fold models developed, ranging from *in vivo* to *in vitro*, from driven models to flow induced vibration models. The sizes of these models have ranged from life size to scaled up models. Each approach has advantages and disadvantages related to accuracy, repeatability, and resolution. But each one has contributed to the current state-of-the-art in understanding phonation.

Excised vocal fold and *in vivo* models have historically been used because they provide anatomically and physiologically accurate models of a highly complex geometry. Khosla *et al.* (2007) used three excised canine larynxes to investigate axial flow during phonation. Physiological variations existed between the larynxes, specifically in the length of the membranous folds. After being harvested from euthanized animals, the larynxes required special treatment and refrigeration and experiments were conducted within twenty-four hours. Additionally, all of the cartilage and soft tissue above the vocal folds were removed to provide an unobstructed view of the vocal folds. Special care was required to attach and prepare the vocal folds in the experimental setup, and humidified air was required for the experiment.

While excised models may include simulated forces exerted by the thyroarytenoid muscle, use of *in vivo* models require no such adjustments. Dollinger *et al.* (2005) used the hemilarynx method in an *in vivo* canine model to quantify the medial surface dynamics of the vocal folds. Surgery and appropriate heating and humidification were required in order to conduct the experiment. Although the hemilarynx method afforded improved optical access over traditional endoscopy, this imaging technique had limited simultaneous access of both the superior and medial surfaces.

Complexities associated with *in vivo* and excised models have led to the use of physical models designed to focus on key aspects of vocal fold motion in repeatable and controllable ways, but using no tissue. However, the challenge of spatial and temporal resolution with geometrically similar models remains. Scaled models have been used. But this approach creates the challenge of preserving physiological accuracy while ensuring dynamic similarity.

Thomson et al. (2005) created complementary physical and numerical vocal fold models with the size, shape, and properties of human vocal folds.

Cohen (2006) developed a compliant, self-oscillating model of the glottis that was geometrically, but not dynamically, similar to physiological conditions. The Digital Particle Image Velocimetry (DPIV) flow measurement technique, first described by Willert & Gharib (1991), and edge detection method developed provided insight into the structural behavior during vibration.

Static physical models have been used to investigate specific configurations of the vocal folds during the oscillation cycle. This approach has several advantages, specifically repeatability and resolution of the data, as well as anatomical similarity. However, the fluid structure interaction dynamics is lost. Symmetric and asymmetric model configurations have been studied in order to investigate the impact of various pathologies on voice production.

Work done by Erath & Plesniak (2006a, 2006b, 2010) explored pulsatile two-dimensional flow through static asymmetric divergent models of the human vocal folds. They used Particle Image Velocimetry (PIV) to compare laryngeal flow to previous studies on symmetric static glottal models, but were unable to model the transition from converging to uniform and diverging glottis because of the static nature of the experiment. The data were used to study the effect of geometric asymmetry on glottal jet stability.

Scherer et al. (2001) developed the static M5 model vocal fold to study symmetric and asymmetric vocal fold configurations. The asymmetric case used both divergent and convergent profile models. A series of pressure taps along the vocal fold surfaces were used to quantify the pressure distribution along each vocal fold.

To overcome some of the limitations of static models, Mongeau et al. (1997) designed a life-sized mechanical model of the human vocal folds which had an opening driven by the two actuating rods embedded in a rubber model. The model was operated over a range of 10 to 150 Hz. The authors stated that while most measurements for maximum glottal area were within 3% of the model parameters, the material choice for the mechanism in addition to inconsistencies with moving mechanism parts introduced variability in the orifice geometry during a cycle. The key variability was an asynchronous glottal opening.

Barry, et al. (2004) developed and tested a driven scaled up model that executed a periodic motion across a model larynx, utilizing the DPIV method to take velocity data. As described in Krane, et al. (2007) and Krane, et al. (2010), the model operated at scaled frequencies ranging from 30 to 130 Hz. These studies showed flow variations that repeatably tracked the gap motion, though some vibration frequency variation was observed. Also observed were fluctuations associated with glottal jet vortical structures, whose phase relative to the gap appeared stochastic. No jet asymmetries were observed for frequencies spanning the range of normal adult phonation. This research studied glottal flow for cases of symmetric motion at different Strouhal and Reynolds numbers. Further work done by Peterson (2007) using the same experimental setup and models investigated asymmetric model behavior to explore conditions of paralysis and paresis. A stepper motor was used to drive the model for both experiments, yielding repeatable results.

Triep, et al. (2005) and Triep & Brückner (2010) developed a driven model to mimic the motion of the vocal folds. The model operated at a scaled frequency to match the average male speaking voice of 120 Hz. The experiment was executed in a water tunnel, and DPIV was used to capture the motion. This research used a driven model to investigate vortex production through the glottis. Two counter rotating elliptical cams were used to approximate the changing glottal profile from divergent to convergent vocal folds during an oscillation cycle.

To further explore the complexities of the flow, specifically to examine the effects of three-dimensionality of the vocal fold geometry, Mattheus & Brückner (2011, 2018) conducted numerical studies of the physical experiments done by Triep & Brückner (2010). They did detailed analysis of the jet structure emanating from the vocal folds over ten successive oscillation cycles and found that there were minimal cycle-to-cycle variations. By this, they concluded that the Coanda effect was not an issue in human phonation.

Kucinshi et al. (2006) developed a driven mechanical model that executes two of the lower order eigenmodes of the vocal folds identified in a computational study by Berry et al. (1994) and Titze & Martin (1998). The model used a deformable latex material stretched across rotating cylinders to approximate the rotation and translation of the vocal folds. The

model size and frequency were scaled, with the Strouhal and Reynolds numbers matched for dynamic similarity.

1.3. Integral Control Volume Analysis and Its Relation to Aeroacoustics

This section provides a brief presentation of the mass and momentum equations written in integral control volume form. This overview follows the analytical development described in Benaroya & Wei (2000) for vortex-induced-vibration of cylinders in a cross flow. For an alternative development focused specifically on the interrelationship between the fluid dynamics and acoustics, the reader is referred to Krane (2013, 2019). In the end, however, the equations are substantively one in the same.

To begin, then, one can examine a flow of interest by defining a finite dimension control volume, *CV*, (as opposed to an infinitesimally small fluid element) that is bounded by a mathematically closed control surface, *CS*. For the glottis, there are open control surfaces at the subglottal and supraglottal ends of the airway. The remainder of the control volume is defined by the walls of the airway itself including the vocal folds. The general mass conservation equation in integral form for this control volume is:

$$\iint_{CS} \rho u_i dS_i + \partial / \partial t \left(\iiint_{CV} \rho dV \right) = 0 \quad [1].$$

Here ρ is the fluid density, u_i is the local fluid velocity vector, dS_i is the differential area element oriented perpendicular to the control surfaces and dV is a differential volume element in the control volume. The subscripts, *CS* and *CV*, denote integration across the control surface and control volume, respectively. This is a statement that the net mass flow across the boundaries of the control volume, *i.e.* the first term of eqn. [1] must be equal and opposite to the rate of change of mass contained inside *CV*. If there were a source or a sink within the control volume, this would no longer be a conservation equation and the right-hand side would contain an expression describing that addition or loss of mass.

In general, the mass of the fluid contained within control volume will change both because of compressibility effects and because of volume changes associated with the wall motion. This rate of change of mass is described by the second term in eqn. [1], For glottal flows, however, the flow is unidirectional in the bulk, and taken to be incompressible, as discussed by Hirschberg (1992). So the continuity equation can be written:

$$\iint_{CS} u_i dS_i = dV / dt \quad [2].$$

Recalling that a monopole source is defined as a time-varying net change in volume, one can see that the right-hand side of eqn. [2] is related to the monopole source strength resulting from vocal fold wall motions.

The integral form of the linear momentum equations is written:

$$\rho \partial / \partial t \left(\iiint_{CV} u_i dV \right) + \iint_{CS} \rho u_i u_j dS_j = - \iint_{CS} p dS_i + \iint_{CS} \tau_{ij} dS_j \quad [3].$$

Observe that the first term in eqn. [3] represents the rate of change of fluid momentum inside the control volume. The second term represents the net momentum flow rate across

the control volume boundaries. The third term is the net pressure force acting across the control volume. And the last term describes the net viscous force acting on the control volume.

Further, observe that each term except the third term, *i.e.* the net pressure force term, can be computed from spatially resolved velocity fields, such as those obtained using DPIV. Computing the residual of the first, second and fourth terms in eqn. [3], then, provides information about the net pressure forces acting in the streamwise and transverse directions. For a description of how these terms were calculated for this particular flow, see Halvorson (2012).

Where continuity relates monopole strength to net volume flux, the momentum equations, in turn, are related to the dipole source strength. Specifically, Krane (2013, 2019) showed that the dipole strength is proportional to the net drag force on the vocal folds (though this is not as immediately obvious from eqn. [3]). Ultimately, quantifying dipole source strength from this approach will require resolution of all four terms in eqn. [3]; one of the key contributions of this paper is developing the capability to do just that.

1.4. Problem Statement

The preceding review highlights the spectrum of experimental methodologies that have been used to study the aerodynamics of human voice. Excised and *in vivo* models provide physiological accuracy but have inherent experimental limitations. Physical models have been developed to overcome these limitations, but they are, conversely, not fully physiologically accurate or complete. Regardless of approach, the challenge remains to make both spatially and temporally resolved measurements of flow past geometrically and physiologically accurate vocal fold models.

One of the long-standing challenges in solving these vexing voice disorders is the ability to accurately model and predict voice production under varying physiological conditions. In particular, understanding the linkages between the aerodynamics and acoustics in the glottal region is particularly problematic. The location and physical dimensions of the glottis make non-invasive measurements virtually impossible, and, limitations in experimental as well as computational methods, continue to plague this field.

In a concurrent effort, Krane (2013, 2019) has been developing a theoretical framework tying the aeroacoustics of phonation with the fluid dynamics of air flowing through the glottis. The framework entails defining an integral control volume bounded by the walls of the glottis and upstream (subglottal) and downstream (supraglottal) control surfaces. With this formation, the integral forms of the mass and momentum conservation equations link the monopole source strength to net changes in glottal volume, and the dipole source strength to the net aerodynamic drag on the vocal folds. In principle, then, if one can obtain time resolved flow measurements of the mass and momentum fluxes across the upstream and downstream control surfaces and the vocal fold motions, one can directly extract information about the sound generated during phonation. There have been other researchers who have used elements of control volume analysis. In particular, in a two part article, Zhao, et al. (2002) and Zhang, et al. (2002) developed a direct Navier-Stokes computational model

to study the aeroacoustics of phonation. As part of their methodology, they used the Ffowcs-Williams Hawking equation to identify form of source mechanisms. In the second article, Zhang, *et al.* (2002a) examined the vortex dynamics associated with flow through an axisymmetric glottal model and computed wall shear stress and pressure distributions along the vocal folds. In an experimental study from the same laboratory with a different lead author, Zhang, et al. (2002), acoustic pressure measurements were made in an axisymmetric orifice flow with varying orifice geometries. In the previously cited work, Thomson, et al. (2005) computed pressure work using a combination of experiments in support of finite element modeling. But in none of these works is there a complete and systematic characterization of the integral control volume equations and the individual terms comprising those equations.

In the current and previous investigations, *i.e.* Barry, et al. (2004) and Krane, et al. (2007, 2010), spatially and temporally resolved measurements were made in a 10x scaled-up *in vitro* vocal fold model. In those studies, the vocal folds were rigid two-dimensional semi-cylindrical structures that moved in and out of a square cross-section glottal model. In the current study, a more complex, two-dimensional vocal fold model was constructed in an attempt to better simulate actual vocal fold motions. The common feature of all of these studies is that, by conducting the experiments in water, dynamic similitude provided 10x spatial resolution and 1500x temporal resolution.

The experiments described in this paper, then, represent advances in both physical model experiments as well as measurement resolution. As noted earlier, the primary goal is advancing the use of spatially and temporally resolved flow measurements in an integral control volume formulation. It was therefore important to use a physical model flow with all of the richness and complexity of flows observed in glottal jet studies in the literature and to then quantitatively assess the dynamic importance of the complexities. The objective of this study, then, was twofold:

- **i.** to design a scaled-up oscillating constriction model that adds complexities observed in vocal fold fluid dynamics, and
- **ii.** to demonstrate the ability to compute key spatially and temporally resolved quantities in the integral control volume formulation that will ultimately connect phonatory aerodynamic features with the acoustics.

2. The Oscillating Constriction Model

Vocal fold motions in the human glottis can be thought of as a combination of a flapping motion, characteristic of reeds, Chang (1994), and the ‘swinging door’ or rocking motion of valves, described in Bach, *et al.* (2002). A schematic sequence of vocal fold motions in one oscillation cycle is shown in figure 1. The vocal folds are indicated with black lines. Their motions are conceptually modeled using a four-bar linkage that is overlaid using green lines.

One cycle incorporates the opening and closing of the vocal folds. As shown in figures 1a–1c, the mechanism, *i.e.* vocal folds, both open and rock downstream in response to the upstream pressure (from the lungs). Note that the vocal folds first open on the upstream side

and then on the downstream side. In figure 1c, the passage is fully open allowing a jet of fluid to form. Once the upstream pressure is released, elasticity of the system then causes the vocal folds to return to the closed position as shown in figures 1d–1f. Again, the upstream vertices lead the motion as the vocal folds both close and rock back upstream to their rest positions. In the actual physiological system, the glottis remains closed for a finite period, nominally equal to the time elapse from figure 1a–1f, while the upstream pressure rebuilds. After that, the cycle repeats.

The computational modeling work of Alipour, et al. (2000) was used as a conceptual framework for experimentally capturing some of the kinematics of this hybrid of opening and rocking motion. They created a finite-element model of human vocal folds assuming vibrations occur in only a single plane. They used physiological material properties and validated their model motions against previous work. In their paper, they showed trajectories of selected nodes in the computational model. The key features, of relevance to this discussion, were that the largest deformations of ~0.2 cm occur towards the downstream region of the model, where the nodes execute a roughly elliptical path in the spanwise direction. Smaller motions of ~0.1 cm occur in the streamwise direction closer to the upstream end of the model.

A stepper motor driven mechanism was used in this study that actuated the two moving vertices in the four-bar linkage shown in figure 1. Details of the design and construction are provided in Sherman (2011). The trajectory of the downstream vertex was chosen to be an ellipse with its major axis predominantly aligned in the transverse direction. The upstream vertex trajectory was modeled as a smaller ellipse aligned in the streamwise direction.

An installation drawing of the constricted duct model is shown in figure 2. Two nominally identical stepper motor driven oscillating constrictions were inserted into a square, 27.3 cm x 27.3 cm, cross-section acrylic duct and positioned 45.7 cm downstream of the duct inlet. The height of each model was 27.3 cm, and the streamwise dimension of the constrictions at the base, *i.e.* the glottal length, L, was 12.75 cm. When closed, each constriction extended 13.7 cm across the duct. The maximum constriction opening at the narrowest point, d, was 2.26 cm.

A schematic drawing of the constriction oscillation mechanism is shown as the inset to figure 2. Motions of the up and downstream vertices (see figure 1) were actuated by gear mechanisms consisting of a spur gear driving two attached linkages. Each mechanism was connected to a central motor drive shaft. To create the constriction, a sheet of thin rubber gasket material was stretched around the two rollers and attached on the duct side-wall.

It should be pointed out here that the oscillations in this experiment were continuous. That is, as soon as the vocal fold models returned to their initial position, a new oscillation cycle began. As noted previously, actual vocal fold vibrations generally include an interval during which the folds are closed. In this work, however, the duration of this interval was zero. As such, while the physiological parallels to vocal fold aerodynamics may be limited, this model is still very useful in the context of demonstrating the value of control volume analysis to complex flows.

3. Experimental Methods

3.1. Definitions of Coordinates and Key Nondimensional Groups

The three coordinate axes, x_1, x_2 and x_3 correspond to the streamwise, spanwise (*i.e.* across the glottis) and transverse directions, respectively. All vector fields presented in this paper have been oriented with the x_1-axis oriented upward positive in the bulk flow direction. All measurements were made in x_1-x_2 planes. Flow is nominally uniform in the x_3-direction.

There are three key non-dimensional groups for this flow. The Reynolds number, Ud/ν is defined using the maximum centerline speed, U, maximum glottal opening, d, and kinematic viscosity, ν. There are two non-dimensional frequencies, or Strouhal numbers, St, commonly used in the voice literature. The first, $St_L = fL/U$, is based on maximum centerline velocity, U, glottal length, L, and oscillation frequency, f. The second dimensionless frequency, $St_d = fd/U$, replaces the glottal length, L, with maximum glottal opening, d. For this paper, St_L will be used following the convention of Hirschberg (1992) and Krane, et al. (2010).

3.2. Measurement Conditions

Four oscillation frequencies were studied at a fixed Reynolds number of 8000. For a steady state jet velocity, *i.e.* for the models held rigidly open, of 35.5 cm/sec and oscillation periods of 30 sec, 15 sec, 10 sec and 7.5 sec, the corresponding Strouhal numbers, St_L, were 0.012, 0.024, 0.036 and 0.048, respectively. For reference, these would be the equivalent of 50 Hz, 100 Hz, 150 Hz and 200 Hz in human phonation. For this study constriction geometry and motions were symmetric about the model centerline (*please see* §3.4.). The laser sheet was positioned along the horizontal mid-plane of the duct so that measurements were made in the horizontal, x_1-x_2, plane.

3.3. DPIV Measurement Technique

Digital Particle Imaging Velocimetry (DPIV) measurements were made in the oscillating constriction model described in the preceding section and illustrated in figure 2. The model was placed in a large free surface water tunnel with a 137 cm (deep) x 122 cm (wide) x 610 cm (long) test section. The maximum flow rate was ~7,600 liters per minute and the flow was uniform to within 2% across the cross section at any streamwise station. The turbulent intensity in the core flow was less than 0.6% of the mean streamwise velocity. The test section walls and floor were glass for full optical access. A detailed description of the tunnel appears in Logory, et al. (1996).

Flow was seeded with 13μm diameter silver coated hollow glass spheres and illuminated with a sheet of light from a pulsed New Wave Solo 120 Nd:YAG laser. Video images were captured using a Redlake Motion Pro X3 b/w digital camera with 1280 x 1024 pixel resolution.

Timing of the constriction stepper motors and image capture system were synchronized using a Berkeley Nucleonics BH-555 pulse delay timing box. For the two lower frequency cases, data were captured at each of the 200 steps in an oscillation cycle. For the two higher

frequencies, data were acquired at every second step. A maximum of 500 successive image pairs could be captured due to limitations of the image acquisition system memory. Multiple runs were conducted to create an ensemble of oscillation cycles at each frequency. For the lower two frequencies, at least seven oscillation periods were recorded. At least fourteen individual oscillation cycles were captured for the two higher frequencies.

3.4. Image Processing

Two-dimensional velocity fields were computed from the video records using an in-house DPIV processing algorithm developed by Hsu (2002). The routine uses a two-stage correlation process, where a coarse velocity field is first calculated and used as input to a fine correlation stage. In this study, the coarse vector field was computed using 128 x 128 pixel interrogation windows followed by 64 x 64 pixel fine correlation windows. Four times over sampling was used so that the spacing between vectors was 16 pixels or ~0.13 cm. A comprehensive uncertainty analysis may be found in Hsu, et al. (2000). The result was a set of time resolved sequences of flow at the different oscillation frequencies. Data were then analyzed using a combination of phase averaging and low pass filtering to examine the coherent structure of flow through the constriction.

A sample vector field overlaid on top of the corresponding video image is shown in figure 3. This is a cropped field taken from one of the $St_L = 0.036$ runs in the jet region. With the laser sheet illuminating the model from downstream, the region shown is that from which the most meaningful data could be extracted. Flow is bottom-to-top with vectors shown in yellow. The bright white curves are the reflection of the pulsed laser sheet on the rubber model walls. Notice the strong jet deflection to the right. As will be discussed in §4, cycle-to-cycle variations in the strength and direction of the jet were oscillation frequency dependent.

In this study, extensive use is made of control volume analysis, where conservation equations are written in terms of a user-defined region through which fluid flows. Here, four connected control surfaces defined by upstream and downstream faces, and right and left constriction surfaces, comprise the control volume. While the upstream and downstream control surfaces are fixed in position with respect to the field of view, the two side control surfaces move with the corresponding constrictions. An edge-detection based wall-tracking algorithm, Halvorson (2012), was developed to identify wall locations in the video images corresponding to each vector field.

Figure 4 is a region of the flow passage between constrictions traced from a single video image. The drawing shows the control volume for this study defined by the closed region, ABCD. The upstream and downstream control surfaces, AB and CD, respectively, are shown as bold black dashed lines. There are, in addition, eight control surfaces inside the control volume shown by lighter weight, grey dashed lines. These were used for volume integral terms in the fluid conservation equations, and for sensitivity analysis. They are spaced ~0.26 cm apart, or two vector spacings in the streamwise direction. Flow is from bottom to top. Note that the upstream control surface, labeled Control Surface #10 in figure 4, was located far enough downstream that there were sufficient vectors in the spanwise direction, even

when the passage was closed, to accurately compute fluid flux terms into the control volume.

3.5. Characterizing Constriction Motions

As will be seen, flow through a nominally symmetric oscillating constriction can be highly asymmetric. As such, it was important to characterize the constriction surface motions to ensure they did not directly cause flow asymmetries. Video records of every oscillation cycle in this study were examined to quantify both cycle-to-cycle repeatability and symmetry of motion. Using edge detection algorithms, the walls of the two moving surfaces were identified in each video frame. From this, time histories of distance between walls at any streamwise location were developed. It was found that for any one frequency, the maximum cycle-to-cycle variation of the constriction at any streamwise location was less than 2%. When comparing the four phase-averaged cycles the maximum variation across the four frequencies was 6%. The repeatability of the oscillations from cycle-to-cycle and across the frequency range was very good.

Next, the symmetry of the two oscillating mechanisms was determined. This was done by finding the locus of mid-points between opposing moving walls at different streamwise locations along the constriction. If the opposing surfaces were perfectly symmetric, the locus of mid-points would be a perfectly straight line aligned in the x_1-direction exactly along the vertical mid-plane of the experiment. This line would not move throughout each oscillation cycle.

Because of the high repeatability of the mechanism motions, it was deemed sufficient to conduct this analysis just for the $St_L = 0.036$ case. It was found that the maximum deviation from a straight line was less than ±0.1 cm and occurred at the downstream end of the constriction. It is important to note that this is <1% of the maximum gap opening at that streamwise location. Symmetry of the experiment, therefore, was also verified.

4. Results and Discussion

4.1. Volume Flow Rate and Maximum Velocity

The simplest integral control volume quantity is net volume flow rate through the constriction. Since there is no flow across the moving side-walls, this is simply the net flow in and out of user defined upstream and downstream control surfaces. A sample downstream control surface is shown as line AB in figure 4. Note that flow upstream of the constriction was not measured.

The volume flow rate across a control surface per unit depth at each instant in time was computed by summing instantaneous streamwise velocity values along that control surface multiplied by the vector spacing. The convention used in this analysis is that volume flow rate is positive outward. Time traces were smoothed using a three-point triangular filter.

Sample time traces of net volume flow rate across control surface, AB, appear in figure 5. This particular example is from the $St_L = 0.036$ case with time, t, normalized by the oscillation period, T. A single trace from one oscillation is shown as a dotted line. The roll-

up of the constriction shear layers into coherent spanwise vortices appears as high frequency oscillations superimposed on the bulk volume flow. By phase averaging over every individual vocal fold oscillation cycle (fourteen for this case) and low-pass filtering, those fluctuations were removed. This phase-averaged, low-pass filtered volume flow rate trace appears in figure 5 as a solid line.

In spite of the repeatability and symmetry of the constriction oscillations, it turns out that there is a high degree of cycle-to-cycle variability in the flow for certain oscillation frequencies. To see these variations, and to examine how integral quantities vary as flow passes along the constriction, three-dimensional surface plots were constructed. This was done by positioning time traces for the six downstream control surfaces, shown in figure 4, along the x_1-axis. Examples are shown in figure 6 for phase-averaged, filtered volume flow rate at $St_L = 0.036$. Plots of maximum velocity and volume flow rate appear in figures 6a and 6b, respectively.

Maximum velocity is defined here as the maximum streamwise velocity value anywhere along a control surface at a given instant in time. This gives the highest speed flow across that control surface at that time irrespective of how symmetric the flow is. One can see in figure 6a, that there is a high degree of cycle-to-cycle variation for the $St_L = 0.036$. That variation is again visible in the volume flow rate data shown in figure 6b.

What is particularly interesting in this figure is the fact that there is a correlation to jet direction as indicated by the letters, ‘L’ and ‘R’ below the surfaces, where ‘left’ and ‘right’ are defined relative to the geometric orientation shown in figure 4. These indicate whether the jet deflected to the left or right as determined by looking at constructions of DPIV vector field video sequences. It was observed that jets that deflect to the right were strong and organized while jets to the left are weaker and less coherent; an example of the jet deflected to the right can be seen in the sample vector field in figure 3. The correlation of jet strength with jet deflection direction is evident in both figure 6a and 6b where the magnitudes of the maximum jet velocity and volume flow rate are smaller when the jet turns to the left than when it turns to the right. This is most noticeable in figures 6 for the control surfaces farthest upstream, *i.e.* the sixth control surface shown in figure 4.

It turns out that this particular frequency exhibited the most switching and the strongest cycle-to-cycle variations in maximum velocity and flow rate. For the lowest frequency, $St_L = 0.012$, no switching was observed with the jet always turning toward the right. For the next highest frequency, $St_L = 0.024$, the first and last jets in the seven oscillations turned to the left, while the other five deflected to the right. And in the highest frequency case, $St_L = 0.048$, over the fourteen consecutive cycles observed, the jet direction would switch every three to four oscillations.

Thus, from a fluid dynamics perspective, there appears to be a strong frequency dependence on the variations with the most variability occurring at $St_L = 0.036$. This may be related to a resonance mis-match between the jet and the model oscillation frequency, *cf.* Benaroya & Wei (2000). To answer this question, however, would require additional detailed study with a significantly larger sample size.

In a phase-averaged sense, however, the differences between oscillation frequency cases is much smaller. Figure 7 shows time traces of phase-averaged, low-pass filtered normalized maximum velocity and volume flow rate for the four frequencies. Each plot is normalized by maximum velocity and flow rate value found over all four cases at that control surface. That is, the maximum velocity of 23.8 cm/s occurring in the $St_L = 0.024$ case was used to non-dimensionalize all four traces in figure 6a and the maximum flow rate of 75.4 cm_2/s, from the $St_L = 0.048$ case was used in figure 7b. Again, time was non-dimensionalized by the corresponding cycle period, T.

One can see in figure 7 that the differences between the four oscillation frequency cases is small, though measurable. It must be kept in mind that the number of cycles in each case, particularly for the two lower frequencies, is relatively small. As such, differences between traces in both figures can likely be attributed as much to small sample size as to any fluid dynamic differences.

4.2 Momentum Balance

Time traces of terms in the streamwise integral momentum equation are shown in figure 8. Each plot includes time resolved traces of inertia, momentum flux, viscous forces and pressure forces. As described earlier, the pressure force term was computed from the residual of the other terms in the momentum balance. While work on direct pressure measurements is ongoing, it should be noted that the pressure at the inlet to the square cross-section duct is constant throughout the oscillation cycles. This was discussed in Krane, et al. (2007) and more recently verified in preliminary measurements presented by Ringenberg, et al. (2018).

Jet deflection directions are again indicated for each oscillation cycle. Data from all four frequency cases are presented using the control volume ABCD indicated in figure 4. As with previous data figures, time is non-dimensionalized by the corresponding oscillation period. The integral momentum terms are presented in their dimensional form with units of gm-cm/s_2. Recall that data for twice as many oscillations were acquired for the higher two oscillation frequencies. Therefore, for comparison purposes, only the first seven of those are presented here so that the nondimensional time axes are the same for all four frequencies.

At the outset, it should be emphasized that the control volume, ABCD, used for this figure encompasses only the jet region of the flow. Consequently, it is not possible to use the current data set for a comprehensive acoustic analysis and modeling effort; this would require direct pressure measurements along the entire model and flow measurements upstream of the model. However, focusing on the jet region, as shown in figures 8, does provide further insights into cycle-to-cycle variations, and the utility of the control volume approach.

The first observation to be made is that, for this particular control volume, the pressure term is roughly equal and opposite to the momentum flux term for all four frequencies. Viscous effects are negligible as would be expected because the side-wall control surfaces, AD and BC, are very short. Additionally, inertia is small compared to the momentum flux and pressure terms.

As discussed in Krane (2013, 2019) and McPhail, et al. (2019), for a full control volume encompassing the entire constriction region, the inertia term should indeed be negligible. There would be, however, a difference between the net streamwise momentum flux and the pressure differential upstream and downstream of the vocal folds. That difference would be equal to the net instantaneous drag on the constriction models. Because of the present focus on the jet region, these questions cannot be addressed here.

The second observation in figure 8 is that the momentum flux and pressure force terms change sign both from cycle-to-cycle but also within individual cycles. For example, for St_L = 0.012 in figure 8a, the momentum flux term is positive during the first ~20% of each cycle and then becomes negative; the pressure force term, of course, does the opposite. While the first and last oscillation cycles in figure 8a are somewhat different, momentum flux and pressure force traces for the second through sixth cycles are very similar. In particular, in each oscillation, there is a positive momentum flux spike with magnitude in the range of 250 – 500 gm-cm/sec_2 lasting ~15 – 20% of the cycle. These are followed by negative momentum flux spikes with magnitudes of ~750 gm-cm/sec_2 lasting roughly half of the oscillation cycle.

Finally, cycle-to-cycle variations are quite apparent in figures 8b–d, particularly in figure 8c, for the St_L = 0.036 case. This is consistent with the observed cycle-to-cycle variations highlighted in figure 6. Here, the pattern of a short duration positive momentum flux spike followed by a longer duration negative momentum flux interval no longer repeats with each cycle. Unlike the maximum velocity and volume flow rate plots shown in figure 6, however, cycle-to-cycle variations of terms in the streamwise integral momentum do not appear to be well correlated with the jet direction.

There are a number of factors that could contribute to the change in sign of these terms. At the beginning and end of each oscillation, there is a small negative volume flux across control surface AB. Given that this control surface is located at the exit plane of the vocal fold models, this negative volume flux is likely due to recirculation associated with remnants of the jet at pinch-off Since the area vector is defined as positive in the outward normal direction, reverse flow would result in a negative momentum flux.

But, most importantly, the momentum flux traces in figure 8 are the *net* flux across surfaces AB *and* CD, *i.e.* across the jet region. As such, it is the difference between the fluxes across the two surfaces. One must then assess what is happening across each surface and ascertain which control surface is contributing more to the net integral. For example, while there may be residual back flow across AB after the glottis closes, when the cycle begins, the start-up jet will first cross control surface CD. For the unit normal sign convention, the start-up jet across CD will be a positive contribution to the *net* momentum flux integral. This brief discussion illustrates that the phase relation between up and downstream control surfaces strongly affect the sign and magnitude of the net momentum flux integral.

It is not possible at this point to ascertain precisely why switching occurred and why traces in figure 8 look the way they do. An additional study is ongoing to specifically examine the effects of asymmetric motions of the two constriction models. What is abundantly clear is

that these phenomena and the methodology to analyze them would not be possible without the spatially and temporally resolved measurements illustrated in this paper.

5. Conclusions

Spatially and temporally resolved measurements have been made of flow in a computer-driven symmetric oscillating constriction. The purpose of this study was to develop noninvasive measurement methodologies as well as the integral control volume analyses necessary to support studies of glottal jet aerodynamics. In so doing, it was important to examine some of the significant asymmetries arising from a nominally symmetric geometry characteristic of these types of flows. Four oscillation frequencies, corresponding to St_L = 0.012, 0.024, 0.036 and 0.048, were examined. The key findings and conclusions from these data were:

- highly asymmetric, time-varying flow phenomena were observed even in a nominally symmetric, highly-repeatable experiment,
- cycle-to-cycle variations, *i.e.* exit jet switching, was strongly dependent on constriction oscillation frequency; the St_L = 0.036 case exhibited the greatest variability,
- spatially and temporally resolved flow measurements allows for the application of integral control volume analysis, a powerful tool for analyzing the dynamics of these complex time-dependent flows; *of particular importance is the ability to non-invasively extract pressure information from flow measurements*,

Examination of flow asymmetries and implementing a control volume that can be directly applicable to acoustic analysis of these flows are the targets for future work.

Acknowledgements:

This work was supported by the National Institutes of Health under grant NIH 2R01 DC005642-14.

References

Alipour F, Berry DA, & Titze IR 2000 A finite-element model of vocal-fold vibration. Journal of the Acoustical Society of America, 108, 3003–3012.

Barry M, Krane M & Wei T 2004 Flow characteristics in a scaled-up glottis model. Journal of the Acoustical Society of America, 115, 2611.

Benaroya H & Wei T 2000 Hamilton's principle for external viscous fluid-structure interaction. Journal of Sound & Vibration, 238, 113–145.

Berry DA, Herzel H, Titze IR, Krischer K 1994 Interpretation of biomechanical simulations of normal and chaotic vocal fold oscillations with empirical eigenfunctions. Journal of the Acoustical Society of America, 95, 3595–3604.

Cohen B 2006 Experimental study of the flow-induced vibration of a flexible duct constriction. M.S. thesis, Dept. Mechanical & Aerospace Eng 'g., Rutgers University, New Brunswick, NJ.

Erath BD & Plesniak MW 2006a An investigation of bimodal jet trajectory in flow through scaled models of the human vocal tract. Experiments in Fluids 40, 683.

Erath BD & Plesniak MW 2006b An investigation of jet trajectory in flow through scaled vocal fold models with asymmetric glottal passages. Experiments in Fluids, 41, 735–748.

Erath BD & Plesniak MW 2010 An investigation of asymmetric flow features in a scaled up driven model on the human vocal folds. Experiments in Fluids, 49, 131–146.

Halvorson LM 2012 Coanda switching phenomena in a nominally symmetric scaled up vocal fold model. M.S. thesis, Dept. Mechanical, Aerospace & Nuclear Eng ‘g., Rensselaer Polytechnic Institute, Troy, NY.

Hirschberg A 1992 Some fluid dynamic aspects of speech. Bulletin de la Communication Parlée, 2, 1–30.

Hsu TY 2002 Hydrodynamic stability at the exit of a papermachine headbox. Ph.D. dissertation, Dept. of Mechanical & Aerospace Eng’g., Rutgers University, New Brunswick, NJ.

Hsu TY, Grega LM, Wei T, & Leighton RI 2000 Turbulent kinetic energy transport in a corner formed by a solid wall and a free surface. Journal of Fluid Mechanics 410, 343–366.

Krane MH, Barry M & Wei T 2007 Unsteady behavior of flow in a scaled-up vocal folds model. Journal of the Acoustical Society of America, 122, 3659–3670.

Krane MH, Barry M & Wei T 2010 Dynamics of temporal variations in phonatory flow. Journal of the Acoustical Society of America, 128, 372–383.

Krane MH 2013 Aeroacoustic sources in phonation: formulation. 10th International Conference Advances in Quantitative Laryngology, 67.

Krane MH 2019 Aeroacoustic sources in phonation: a control volume approach. Journal of the Acoustical Society of America (in review).

Kucinschi BR, Scherer RC, DeWitt KJ & Ng TM 2006 An experimental analysis of the pressure and flows within a driven mechanical model of phonation. Journal of the Acoustical Society ofAmerica, 119, 3011–3021.

Logory LM, Hirsa A & Anthony DG 1996 Interaction of wake turbulence with a free surface. Physics of Fluids, 8, 805–815.

Mattheus W & Brücker C 2011 Asymmetric glottal jet deflection: differences of two-and three-dimensional models. Journal of the Acoustical Society of America, 130, 10.1121/1.3655893.

Mattheus W & Brücker C 2018 Characteristics of the pulsating jet flow through a dynamic glottal model with a lens-like constrictions. Biomedical Engineering Letters, 8, 309–320. [PubMed: 30603215]

McPhail M, Campo E, and Krane M 2019. Aeroacoustic source characterization in a physical model of phonation, in press, Journal of the Acoustical Society of America.

Mongeau L, Francheck N, Coker CH, & Kubli RA 1997 Characteristics of a pulsating jet through a small modulated orifice, with application to voice production. Journal of the Acoustical Society of America, 102, 1121–1133.

Pelorson X, Hirschberg A, van Hassel RR & Wijnands APJ 1994 Theoretical and experimental study of quasisteady-flow separation within the glottis during phonation: Application to a modified two-mass model. Journal of the Acoustical Society of America, 96, 3416–3431.

Peterson K 2007 Experimental Investigation into the aerodynamic consequences associated with dysphonic conditions. M.S. thesis, Dept. Mechanical, Aerospace & Nuclear Eng’g., Rensselaer Polytechnic Institute, Troy, NY.

Ramig LO & Verdolini K 1998 Treatment efficacy: Voice disorders. Journal of Speech, Language, and Hearing Research, 41, S101–S116.

Ringenberg H, Rogers D, Wei N, Krane M & Wei T 2018 Pressure-velocity correlations in a scaled up vocal fold model – symmetric case. Bulletin of the American Physical Society, 62, 260.

Roy N, Merrill RM, Gray SD, & Smith EM 2005 Voice disorders in the general population: Prevalence, risk factors, and occupational impact. The Laryngoscope, 115, 1988–1995. [PubMed: 16319611]

Scherer RC, Shinwari D & DeWitt KJ 2001 Intraglottal pressure profiles for a symmetric and oblique glottis with a divergence angle of 10 degrees. Journal of the Acoustical Society of America, 109, 1616–1630.

Sherman E 2011 Investigation of dysphonic phonation using physiologically similar vocal fold models. M.S. thesis, Dept. Mechanical, Aerospace & Nuclear Eng’g., Rensselaer Polytechnic Institute, Troy, NY.

Tarnopolsky AZ, Fletcher NH & Lai JCS 2000 Oscillating reed valves - An experimental study. Journal of the Acoustical Society of America, 108, 400–406.

Thomson SL, Mongeau L & Frankel SH 2005 Aerodynamic transfer of energy to the vocal folds. Journal of the Acoustical Society of America, 118, 1689–1700.

Titze IR & Martin DW 1989 Principles of voice production. Journal of the Acoustical Society of America, 104, 1148.

Triep M, Brücker C & Schroder W 2005 High-speed PIV measurements of the flow downstream of a dynamic model of the human vocal folds. Experiments in Fluids, 39, 232–245.

Triep & Brückner 2010. Three-dimensional flow nature of the supraglottal jet. Journal of the Acoustical Society of America, 127, 1537–1547.

Willert CE, & Gharib M 1991 Digital particle image velocimetry. Experiments in Fluids, 10, 181–193.

Yang J, Yu F, Krane M & Zhang L 2018 The Perfectly Matched Layer absorbing boundary for fluid-structure interactions using the Immersed Finite Element Method. Journal of Fluids and Structures, 76, 135–152. [PubMed: 29151673]

Yang J, Wang X, Zhang L & Krane M 2017 Fully-Coupled Aeroelastic Simulation with Fluid Compressibility - for Application to Vocal Fold Vibration. Computer Methods in Applied Mechanics and Engineering, 315, 584–606. [PubMed: 29527067]

Zhang C, Zhao W, Frankel SH & Mongeau L 2002 Computational aeroacoustics of phonation, Part II: Effects of flow parameters and ventricular folds. Journal of the Acoustical Society of America, 112, 2147–2154.

Zhang LT & Yang J 2016 Evaluation of aerodynamic characteristics of a coupled fluid-structure system using generalized Bernoulli's principle: An application of vocal folds vibration. Journal of Coupled Systems and Multiscale Dynamics, 4, 241–250. [PubMed: 29527541]

Zhang L, Krane M & Yu F 2019 Modeling of slightly-compressible isentropic flows and compressibility effects on fluid-structure interactions. Computers and Fluids, 182, 108–117. [PubMed: 31327880]

Zhang Z, Mongeau L & Frankel SH 2002 Experimental verification of the quasi-steady approximation for aerodynamic sound generation by pulsating jets in tubes. Journal of the Acoustical Society of America, 112, 1652–1663.

Zhao W, Zhang C, Frankel SH & Mongeau L 2002 Computational aeroacoustics of phonation, Part I: Computational methods and sound generation mechanisms. Journal of the Acoustical Society of America, 112, 2134–2146.

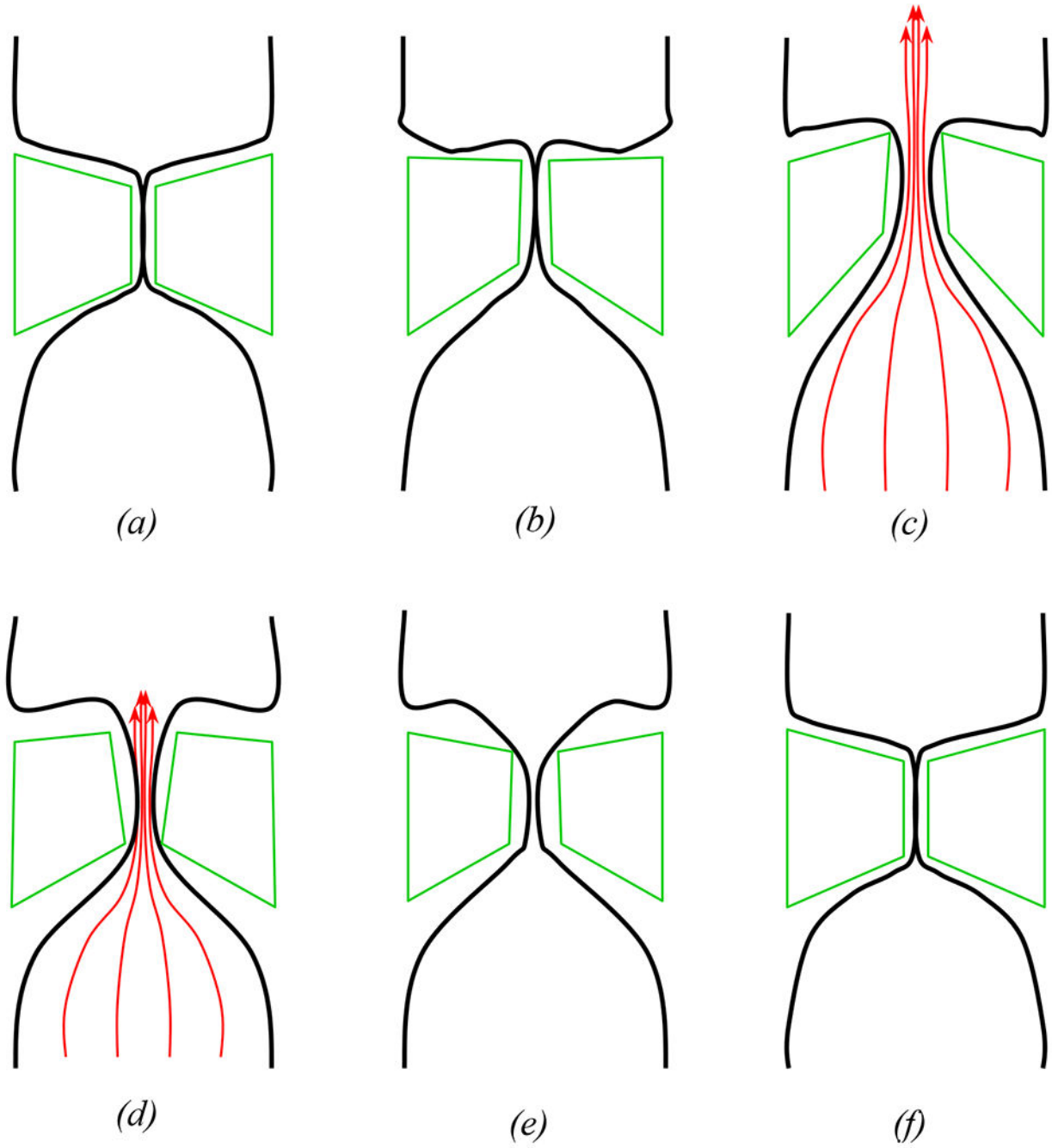

Figure 1:
Simplified schematic of the vocal fold motion. Four bar linkages, in green, are laid over a diagram showing the opening ($a-c$) and closing ($d-f$) phases of one vocal flow oscillation cycle. The red arrows denote airflow up through the glottis when it is open.

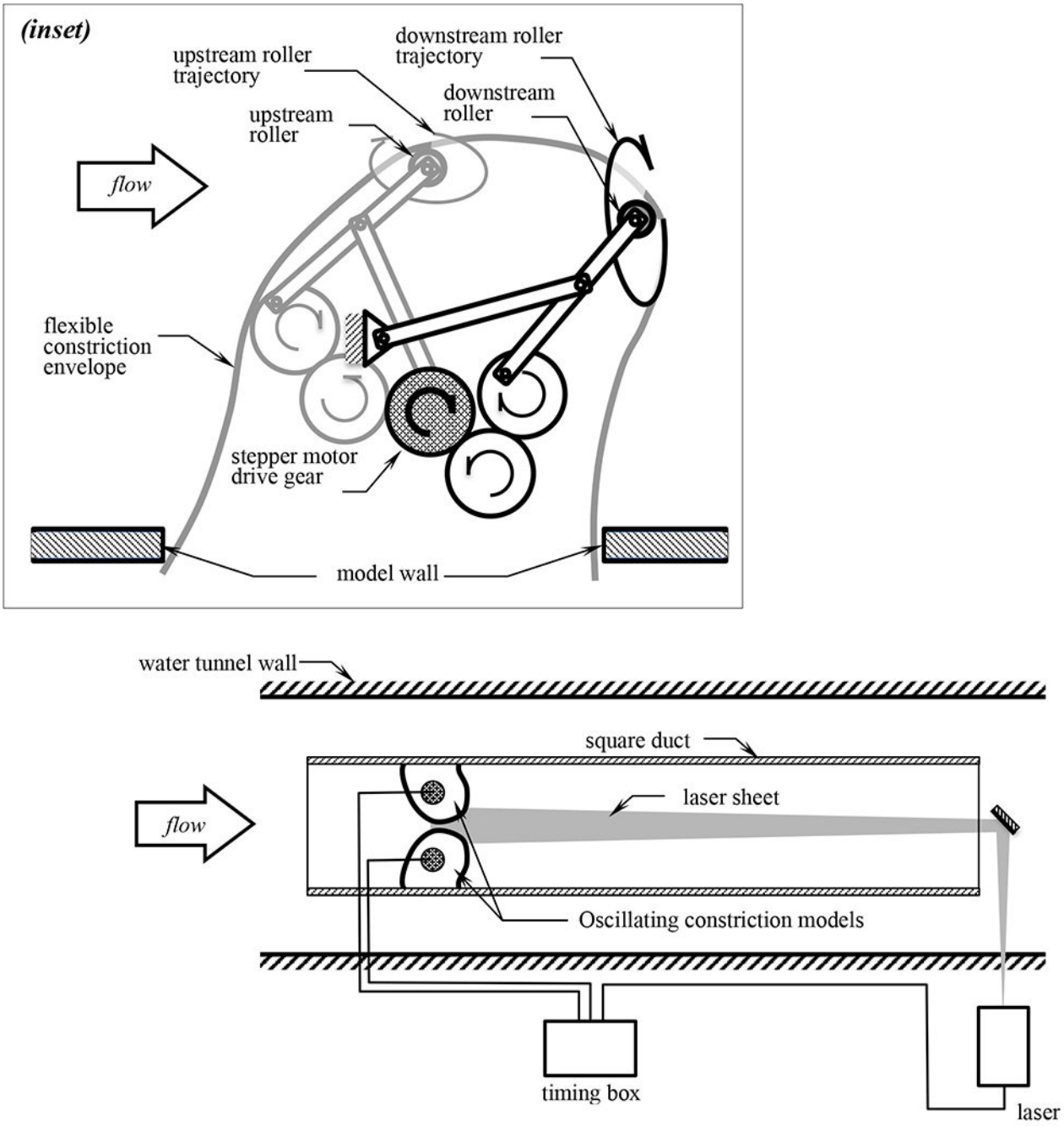

Figure 2:
Plan view schematic of the oscillating constriction experiment. The video camera (not shown) is positioned looking up from below. The two shaded circles represent the stepper motors that drive the constriction models. The inset shows the oscillating constriction mechanism roughly replicating motions of the linkage vertices shown in figure 1. The elliptical arrows indicate trajectories of the two rollers defining the constriction motions.

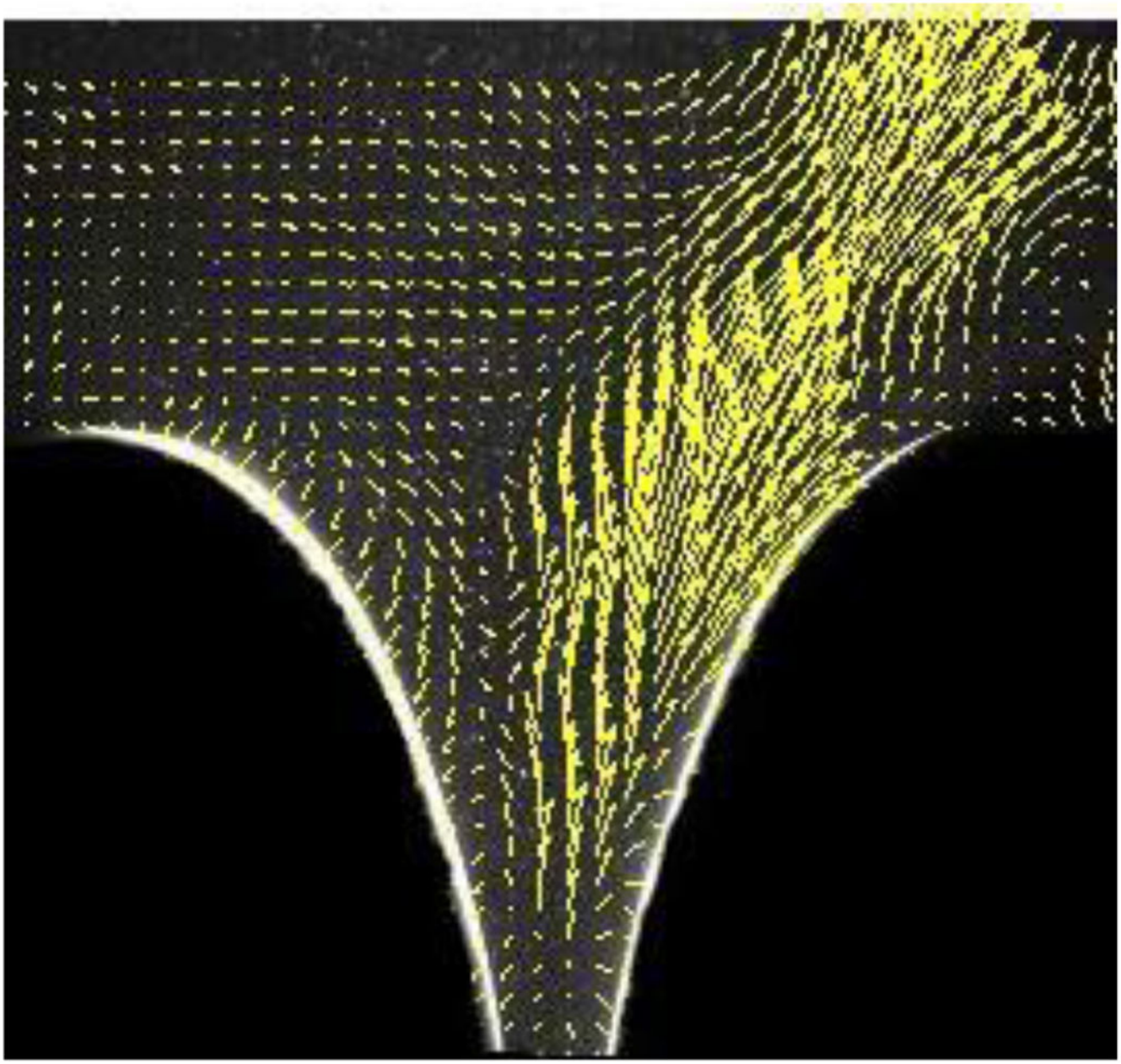

Figure 3:
Sample DPIV vector field overlaid on the corresponding raw video image. The field of view is in the $x_1 - x_2$ plane with the mean flow, x_1-direction oriented from bottom-to-top. Note that only the jet region is shown; the bright white curves are the reflection of the pulsed laser sheet on the walls for the oscillating constriction models. Observe in this image, there is a strong jet flow to the right.

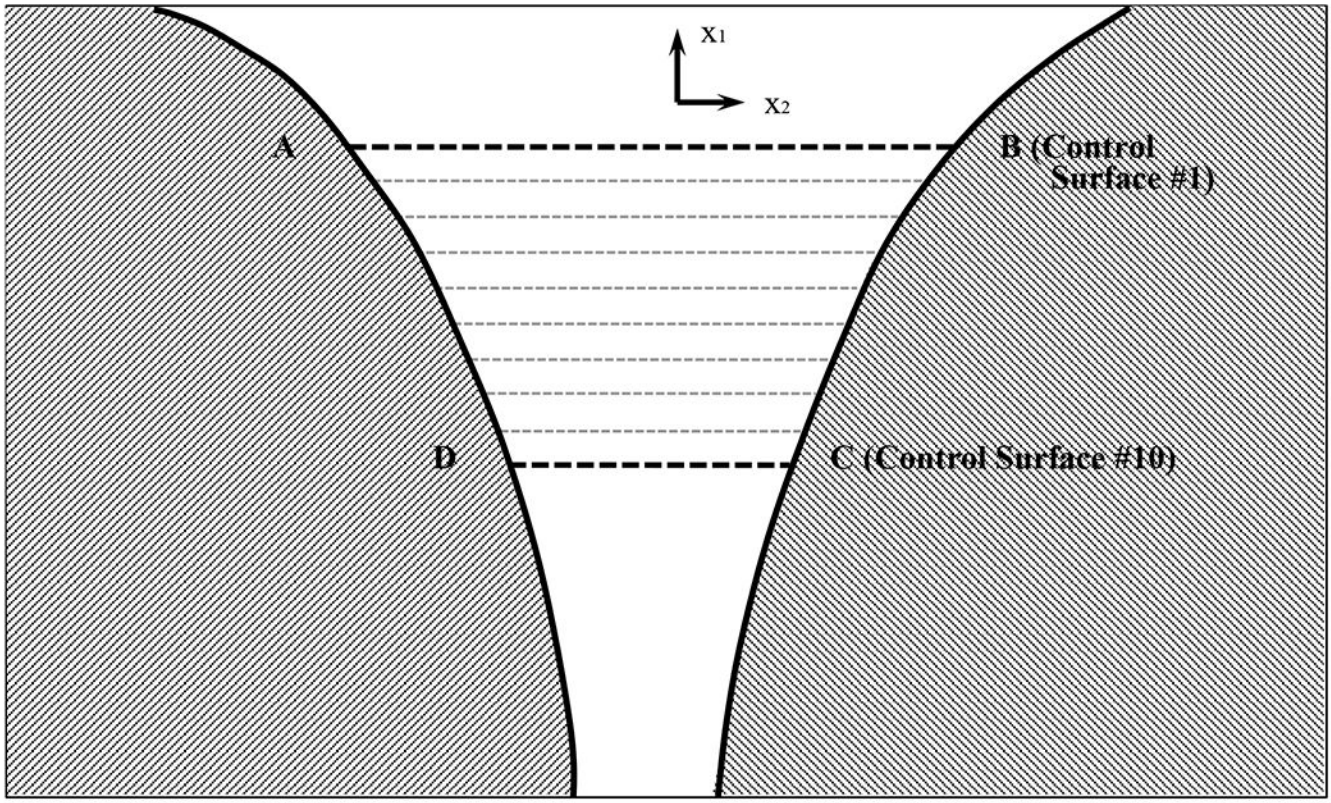

Figure 4:

Line tracing from a video frame showing the downstream portion of flow passage between constriction models (shaded regions). Flow is from bottom to top. The control volume used in this study is indicated by the vertices ABCD. The heavy dashed horizontal lines denote the upstream and downstream control surfaces while the lighter weight grey dashed lines are eight interior control surfaces.

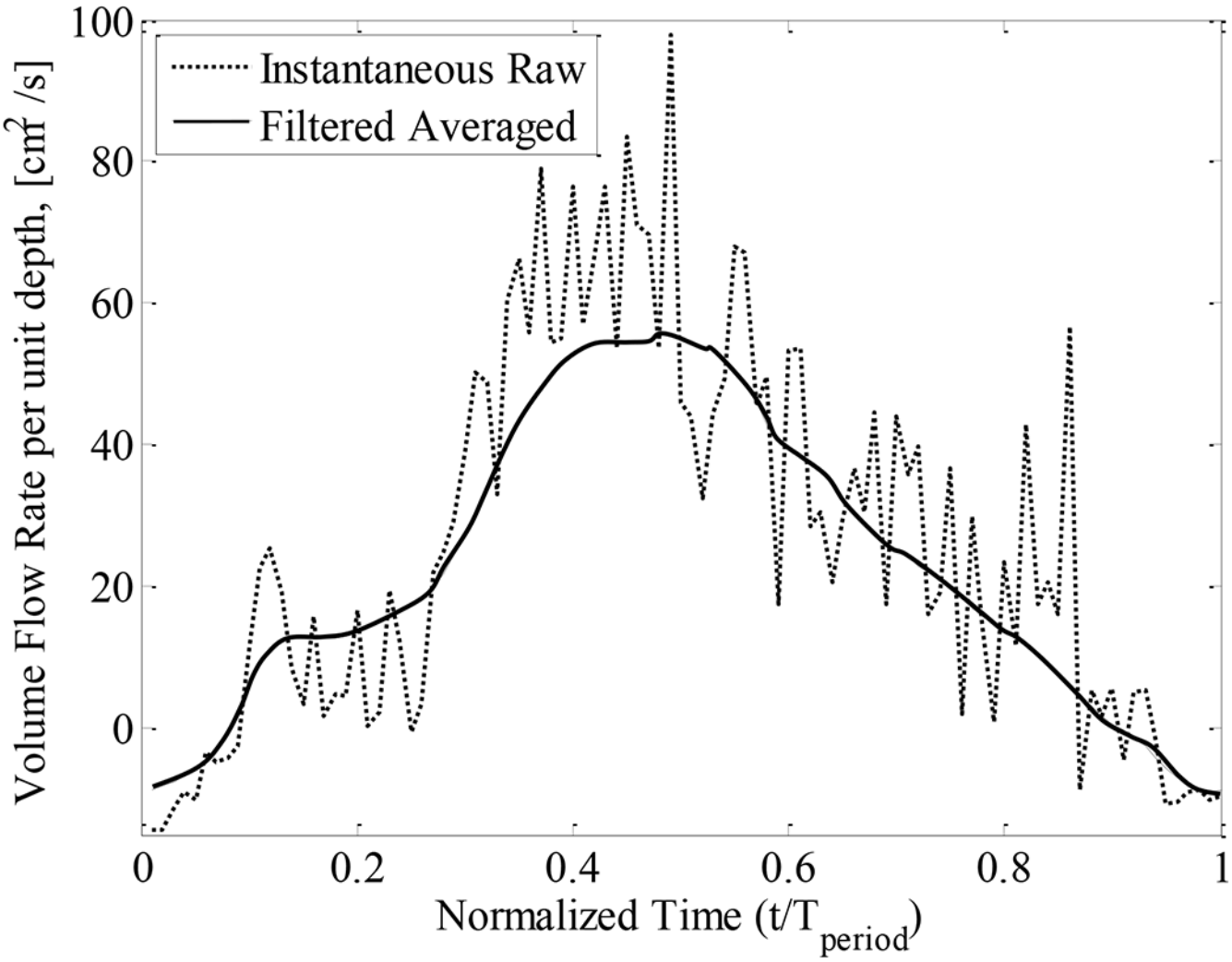

Figure 5:

Time traces of flow rate during a single constriction oscillation cycle in the f^* = 0.0317 case. An instantaneous raw oscillation is shown as the dotted line. The solid line was computed by phase averaging over the fourteen individual oscillation cycles and subsequent low pass filtering.

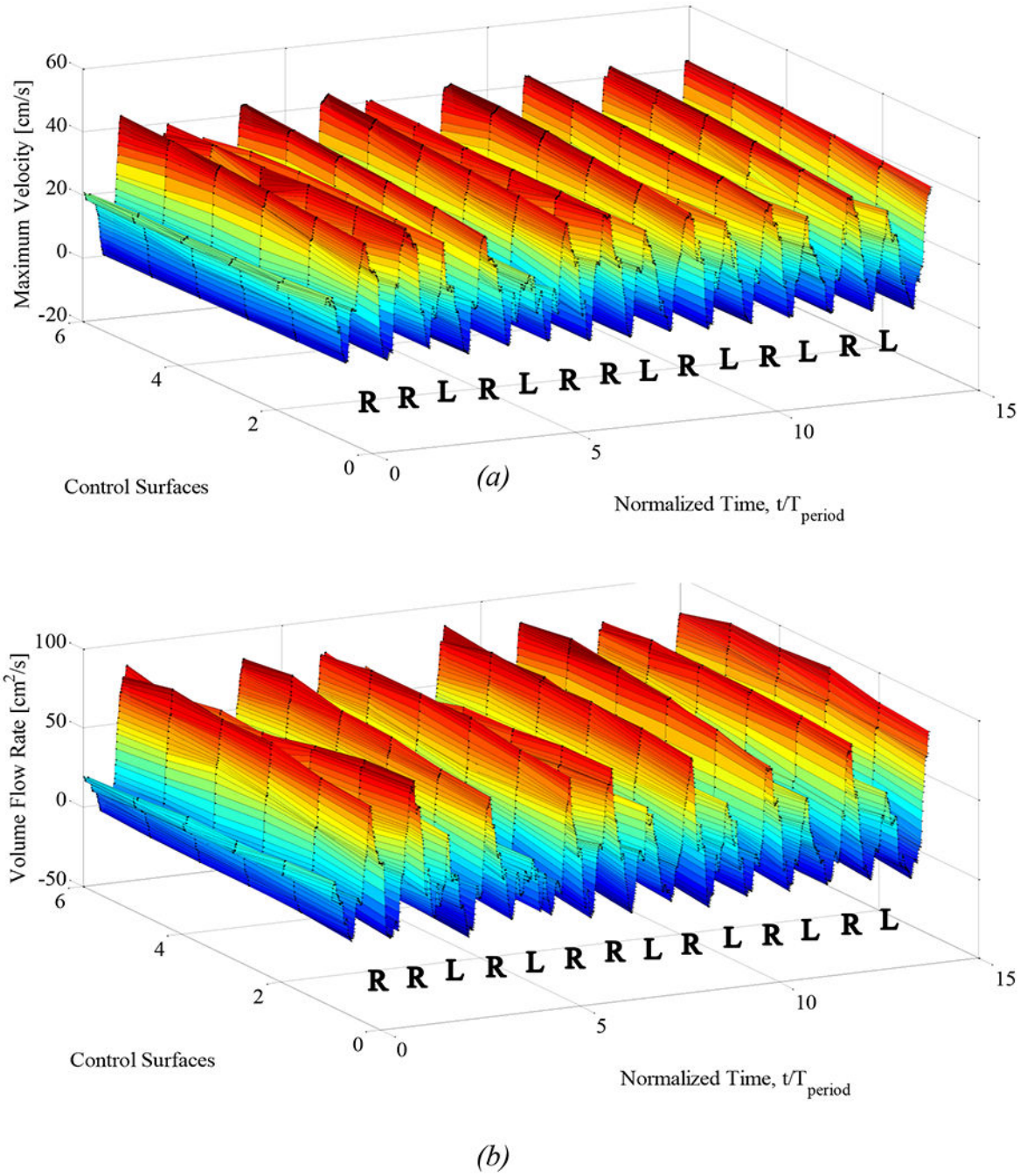

Figure 6:

Surface plots of maximum velocity (*a*) and volume flow rate (*b*) for $f^* = 0.0317$. Both plots were constructed using time traces from each of the six downstream-most control surfaces (*cf.* figure 4). The 'maximum velocity' is the largest streamwise velocity value along the control surface of interest at a given time. The volume flow rate values were computed by integrating the spatially filtered streamwise velocity distribution along the control surface.

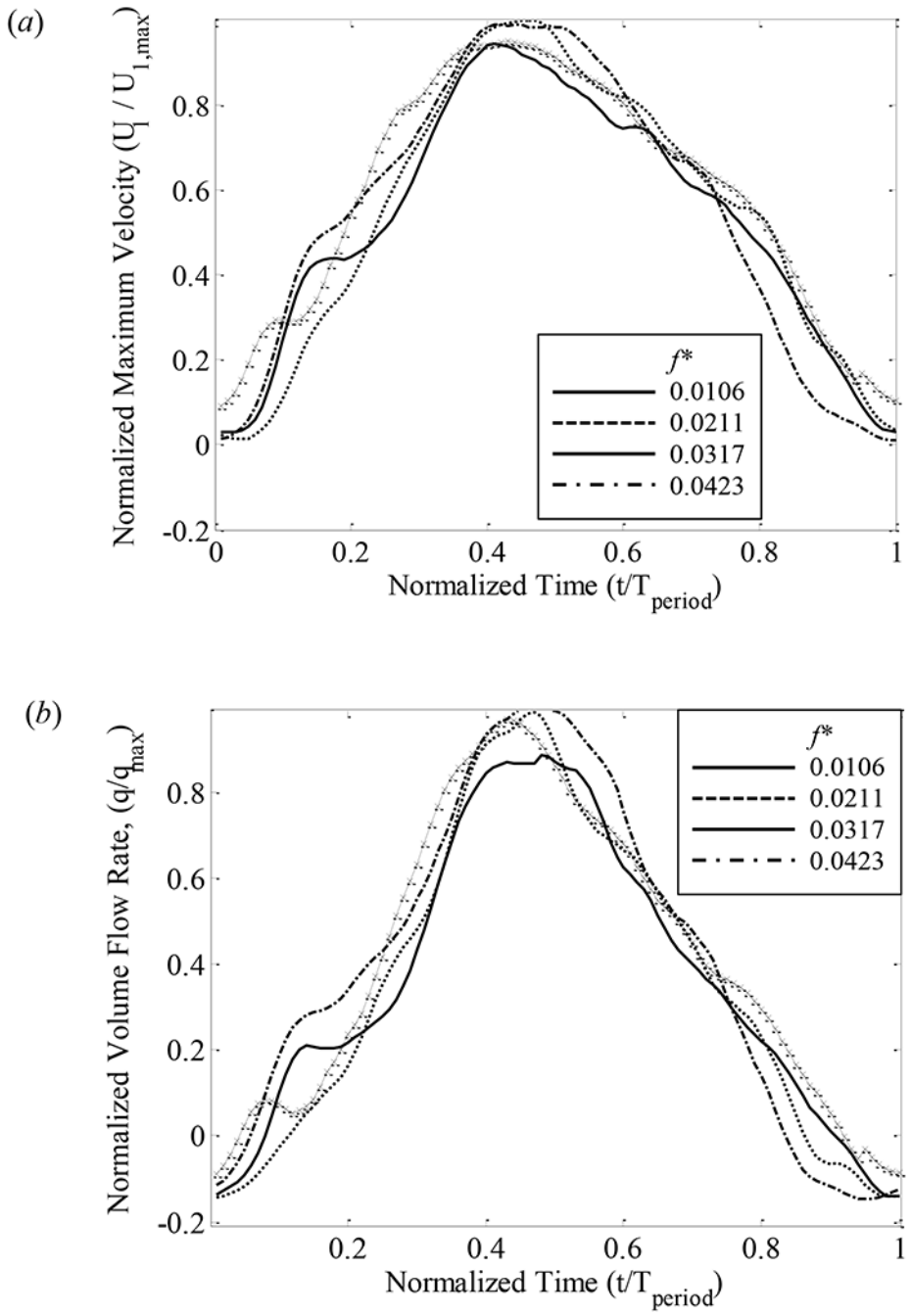

Figure 7:
Normalized maximum velocity (*a*) and volume flow rate (*b*) for the four reduced frequency cases.

(a)

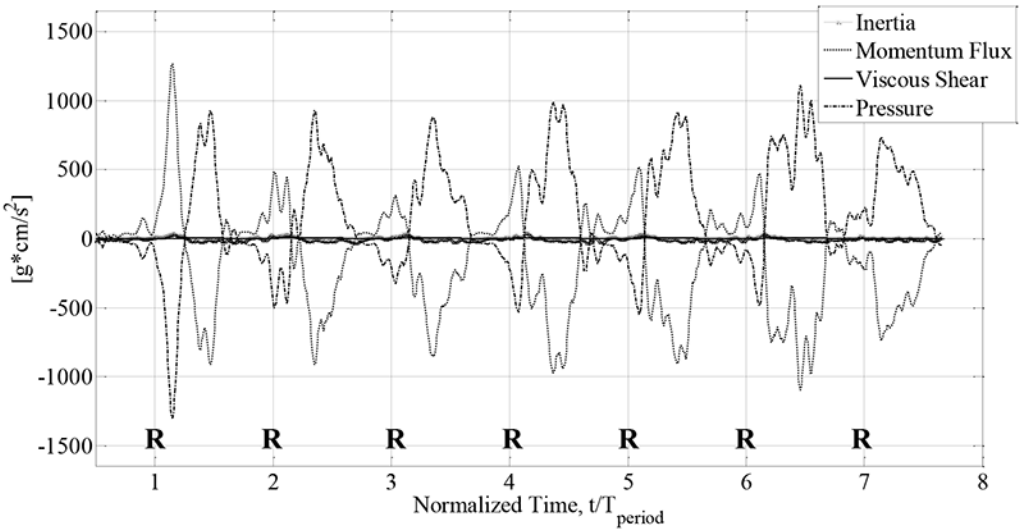

(b)

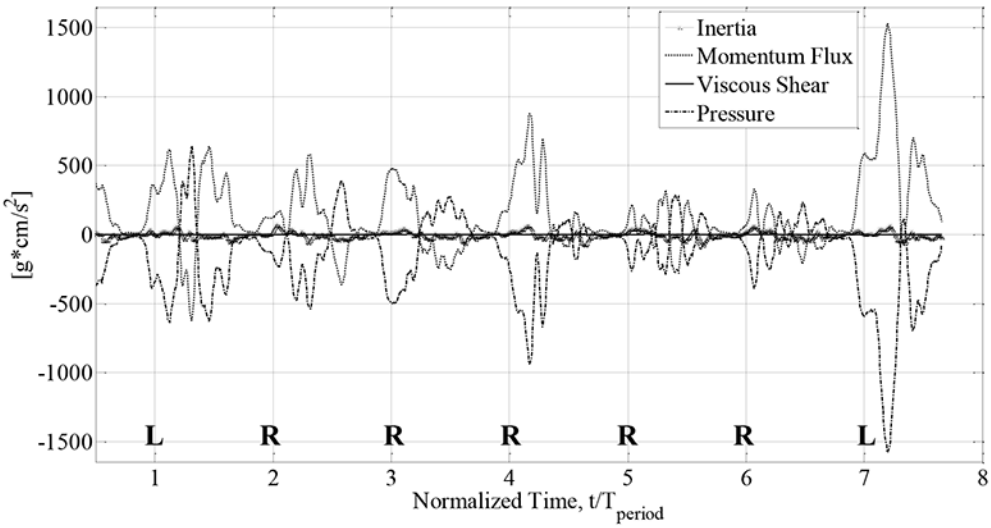

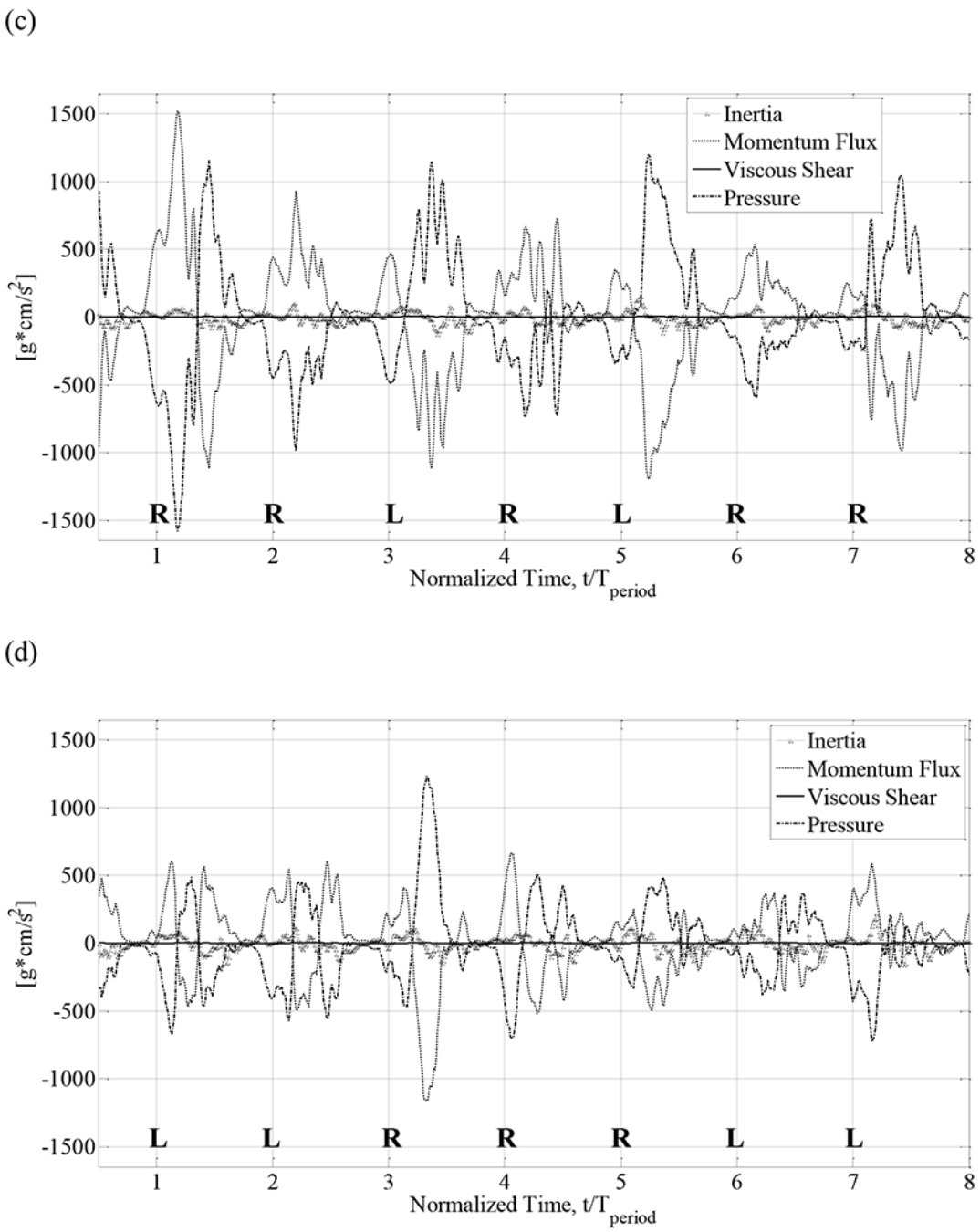

Figure 8:

Time traces of terms in the streamwise integral momentum equation for the four reduced frequencies: (*a*) 0.0106, (*b*) 0.0211, (*c*) 0.0317 and (*d*) 0.0423.